






Article

Electrophoretic Coating of Octahedral Molybdenum Metal Clusters for UV/NIR Light Screening

Thi Kim Ngan Nguyen ^{1,2,3} , Benjamin Dierre ³, Fabien Grasset ^{2,3} , Noée Dumait ⁴, Stéphane Cordier ⁴ , Pierric Lemoine ⁴, Adèle Renaud ⁴, Hiroshi Fudouzi ², Naoki Ohashi ^{2,3}  and Tetsuo Uchikoshi ^{1,2,3,*} 

¹ Graduate School of Chemical Sciences and Engineering, Hokkaido University, Sapporo 060-0808, Japan; NGUYEN.Thikimngan@nims.go.jp

² Research Center for Functional Materials, National Institute for Materials Science, Tsukuba 305-0047, Japan; GRASSET.Fabien@nims.go.jp (F.G.); fudouzi.hiroshi@nims.go.jp (H.F.); ohashi.naoki@nims.go.jp (N.O.)

³ Laboratory for Innovative Key Materials and Structures, UMI 3629 CNRS-Saint Gobain-NIMS, NIMS, Tsukuba 305-0051, Japan; dierre.benjamin@yahoo.com

⁴ Institute of Chemical Sciences of Rennes, UMR 6226 CNRS-University of Rennes 1, Rennes 35000, France; noee.dumait@univ-rennes1.fr (N.D.); stephane.cordier@univ-rennes1.fr (S.C.); pierric.lemoine@univ-rennes1.fr (P.L.); adele.renaud@cnrs-imn.fr (A.R.)

* Correspondence: uchikoshi.tetsuo@nims.go.jp; Tel.: +81-29-859-2460

Received: 22 May 2017; Accepted: 30 July 2017; Published: 3 August 2017

Abstract: Thin and transparent Mo₆ cluster films with significant optical properties were prepared on indium tin oxide (ITO)-coated glass plates from the suspension of Cs₂Mo₆Br₁₄ cluster precursors dispersed in methyl-ethyl-ketone (MEK) by an electrophoretic deposition (EPD) process. Two kinds of polydimethylsiloxanes (PDMS); i.e., KF-96L-1.5CS and KF-96L-2CS corresponding to the kinetic viscosity of 1.5 and 2 centistokes, respectively, were selected to topcoat the Mo₆ cluster film after the EPD. The influence of the PDMS on the durability, chemical compatibility and light absorption property of Mo₆ cluster films were characterized by means of field-emission scanning electron microscopy (FE-SEM), energy dispersive spectroscopy (EDS), Fourier transform infrared spectroscopy (FT-IR), and ultraviolet-visible-near infrared (UV-Vis-NIR) spectroscopy. The stabilized PDMS-coated Mo₆ cluster film could be stored for more than 6 months under ambient conditions.

Keywords: electrophoretic deposition; molybdenum octahedral cluster; methyl-ethyl-ketone; polydimethylsiloxane; UV/NIR absorption

1. Introduction

In recent years, inorganic or organic material-coated glasses exhibiting several special characteristics, such as self-cleaning [1,2], blocking UV-NIR light or generating an electrochromic property [3,4] for a window application, have been intensively studied in order to optimize the specific characteristics and reduce the production costs [5]. The conversion of solar energy to electricity or heat would be an important solution to the energy crisis if hydrocarbon resources, such as coal and other fossil fuels, cannot satisfy the increasing energy demand. Metallic plasmonic nanostructures have been the focus for light trapping in energy-harvesting devices due to the processability in fabricating thin films, improving the light absorption and enhancing the pathway of light by scattering and reflecting between metallic layers [6]. The [Mo₆B₈L₆^a]²⁻ octahedral molybdenum cluster precursors (i = inner ligands, a = apical ligands; L = I, Cl, Br, OH, OCOC₂F₅ . . .) [7,8], have also been studied as light-harvesters in inorganic solar cells [9,10] or LED devices [11]. Considering the ability of light absorption at a wavelength in the UV-visible light range (under 580 nm) and the strong emission

at wavelengths between 600 and 700 nm [12], the octahedral molybdenum nanocluster precursor ($[\text{Mo}_6\text{Br}_8\text{L}_6]^{2-}$) has recently been the focus of attention for the application as a glass coating.

Numerous chemical solution deposition (CSD) techniques [13,14] and physical deposition techniques including sputtering and pulsed laser deposition (PLD) [15], which enable the fabrication of nano/micrometer-thick films, have been used in many fields to functionalize the surfaces of a variety of materials. For example, the PLD process is a versatile coating technique to fabricate thickness and nanostructure-controlled films with less contamination on a substrate [16,17]. Electrophoretic deposition (EPD) is also a promising room temperature process which exhibits the capability to coat thin/thick films in ambient atmosphere on complex-shaped substrates such as tube, sphere and wire netting [18] and the applicability to any suspensions containing charged particles, i.e., conductive polymers [19], organic, inorganic, or organic-inorganic composites [20,21]. The effective application of the EPD process has been extensively studied for the fabrication of traditional ceramic materials for a long time [22,23]. In recent studies, the EPD process has been extended to graphene-related materials [24], nanoscale TiO_2 [25], or medical materials, i.e., antimicrobial applications [26], bond tissue engineering [27], protein identification [28], and bio-implants [29], based on the possible control of the thickness on a nanometer scale.

According to a recent report, the transparent film based on the $[\text{Mo}_6\text{Br}_8(\text{OCOC}_2\text{F}_5)_6]^{2-}$ cluster units, zinc oxide, and polyvinylpyrrolidone (PVP) was successfully fabricated on normal glass by dip coating. However, one strong restriction of this method is the requirement of a high concentration of the polymer matrix in order to stabilize enough Mo_6 clusters on the glass surface [30]. In order to overcome this problems, our previous study investigated the processability of the octahedral Mo_6 cluster film by the EPD process by dissolving the Mo_6 cluster precursors ($\text{Cs}_2\text{Mo}_6\text{Br}_8\text{Br}_6^a$) in different liquid media [31] and concluded that the MEK solution was the most suitable medium in order to obtain transparent, homogeneous, and thin Mo_6 films. The strong advantage of the EPD process is that we can easily fabricate the pure Mo_6 cluster film containing no counter cations at room temperature that create a new Mo_6 cluster network exhibiting prominent luminescent stabilization [31]. The key work is to fabricate the Mo_6 cluster film with no counter cations by depositing the $[\text{Mo}_6\text{Br}_8\text{Br}_{6-x}^a]^{x-2}$ ($\text{L} = \text{H}_2\text{O}$ or OH) anion on ITO conductive substrate by applying an electric field [32]. The crucial characteristic of the Mo_6 octahedral structure is to transfer and store excited electrons in order to prolong the lifetime of the excitation state, besides the absorption of the UV light. The possibility of the transformation and retention the excited electrons properly depends on the distance of Mo-Mo bonding and Mo- X^{inner} -Mo bonding [33]. Therefore, the Mo_6 film without counter cations by EPD process is expected to improve the lifetime of the excitation electrons in the new crystallographic network.

Though the deposition process seemed to be fairly good, the Mo_6 film was obviously cracked within a short time during the evaporation of the solvent. Considering the applications of PDMS successfully studied in many application areas [34], the PDMS coating was carried out as a post treatment of the Mo_6 cluster films after the EPD. The protective mechanism of the PDMS towards the Mo_6 cluster film has also been suggested by the crosslinking reaction between apical ligands of the Mo_6 cluster and the PDMS fluid with low viscosity during the slow evaporation. In fact, the Mo_6 film can be significantly stabilized at thin thickness by the hydrogen bonds generated by OH groups on the ITO glass and OH or H_2O groups on the Mo_6 cluster, but the optical effectiveness is limited with low Mo_6 cluster concentration. This has been proved for a Br-rich cluster layer formed at the initial deposition stage in the previous report [32]. Therefore, it is necessary to fabricate thick and stable Mo_6 cluster film, which is sustainable under ambient condition in order to extend the application of the Mo_6 cluster on window for cutting UV/NIR light. The key work is to figure out a simple and effective coating process to protect the original octahedral cluster structure which contributes to its unique optical properties.

2. Materials and Methods

2.1. Preparation of the EPD Suspension

The $\text{Cs}_2\text{Mo}_6\text{Br}_{14}$ cluster precursor was synthesized at a high temperature by the solid chemistry method from MoBr_2 and CsBr agents [35] (Figure 1a,b). The nanocluster powder was added to reagent grade MEK (99%, Nacalai Tesque, Inc., Kyoto, Japan) at a concentration of 5 g/L, then stirred until obtaining a transparent yellow suspension (Figure 1c) [31]. The zeta potential and electronic conductivity of the prepared $\text{Cs}_2\text{Mo}_6\text{Br}_{14}$ cluster suspension were measured by a zeta-potential analyzer (Zetasizer Nano Z, Malvern Instruments Ltd., Malvern, UK), which were about $-(10 \pm 2)$ mV and (0.32 ± 0.70) mS/cm, respectively. The EPD system was set up as shown in Figure 1d. The SourceMeter (Model 2400, Keithley Instruments Inc., Solon, OH, USA) was connected to a stainless steel cathode and ITO glass (Geomatec Co., Ltd., Tokyo, Japan; $6.15\text{--}7.27 \Omega/\text{sq}$) anodic substrate. The Mo_6 nanoclusters were deposited on the ITO glass ($1 \times 1.5 \text{ cm}^2$) at the applied voltages from 10 to 16 V for 60 s.

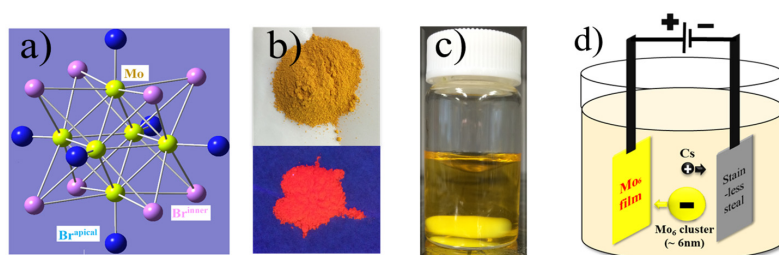


Figure 1. Photographs and schematic illustrations showing the experimental setup: (a) chemical structure of the Mo_6 cluster; (b) as prepared the $\text{Cs}_2\text{Mo}_6\text{Br}_{14}$ powder with and without irradiation at 324 nm wavelength of UV light; (c) suspension of the $\text{Cs}_2\text{Mo}_6\text{Br}_{14}$ powder in MEK solution; (d) EPD apparatus, diameter of the Mo_6 cluster is about 6 nm [32].

2.2. Preparation of the Mo_6 Film Incorporated with PDMS

2.2.1. Hydrophilization of the ITO Glass

The Mo_6 cluster film prepared by the EPD process showed a good transmittance, homogeneity and smooth surface (Figure 2a). However, the surface of the Mo_6 film was easy to break into flakes originating from its edge after drying in the air for 4 days at room temperature (Figure 2b). In order to improve the interaction between the Mo_6 film and the ITO surface, a hydrophilic plasma treatment of the ITO surface was performed by a plasma ion bombarder (PIB-10, Vacuum Device Co., Ltd., Mito, Japan) with a discharge current of 10 mV and a processing time of 3 min (Figure 2c). The hydrophilized ITO glasses showed much better adhesion of the Mo_6 film after the EPD (Figure 2d), but the film still cracked after 9 days.

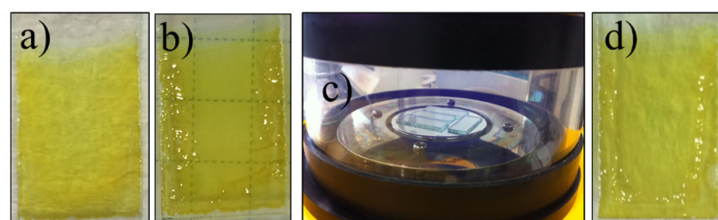


Figure 2. Photographs showing the influence of hydrophilic plasma treatment of the ITO surface on the adhesion of the Mo_6 cluster films: (a) Mo_6 film on the untreated ITO glass just after the EPD (similar image are obtained on plasma-treated ITO glass); (b) after 4 days; (c) the plasma treatment of the ITO glass and (d) Mo_6 film on the plasma-treated ITO glass after 9 days.

2.2.2. PDMS Coating on the Mo₆ Film

Several kinds of PDMSs commercially labeled as KF-96L-*n*CS (*n* = kinetic viscosities; 1.5, 2, 5, 10, 20, and 100; CS = centistokes) were used for the post surface-coating treatment. The viscosity of the PDMS fluids depends on the molecular weight and they contain no solvent. The PDMS with the volume of 0.5 ml was immediately dropped on the surface of the deposited Mo₆ cluster film after the EPD process. In order to apply a similar drying condition, all the PDMS-coated films were dried at 40 °C for 7 days in oven. Moreover, the waiting time to drop the PDMS fluid was investigated in order to obtain good quality film.

2.2.3. Characterization of the Mo₆ Film

The Mo₆ cluster films prepared on the hydrophilized ITO glass (Mo₆ film), then coated with KF-96L-1.5CS (Mo₆ film_1.5CS) or KF-96L-2CS (Mo₆ film_2CS) after 90 min of drying were characterized. The thickness of the films fabricated at the different deposition times and applied voltages was measured by a high-resolution color 3D laser microscope with a 408-nm wavelength laser light. The surface morphology and chemical component of the thin films were observed by field-emission scanning electron microscopy (FE-SEM) (S-4800, Hitachi High-Tech. Corp., Tokyo, Japan) coupled with energy dispersive spectroscopy (EDS). The structural identification of the films was determined by X-ray diffraction (XRD) (SmartLab, Rigaku Corp., Tokyo, Japan) with the tube voltage/current of 40 kV/30 mA in the 2θ angle range from 5° to 35° at the scan speed of 1°/min using Cu Kα radiation (λ = 1.54 Å). The new interaction appearing in the PDMS-coated film was characterized by Fourier transform infrared spectroscopy (FT-IR) (Nicolet 4700, Thermo Electron Corp., Madison, WI, USA) in the wavenumber range from 4000 to 400 cm⁻¹. Optical absorbance of the Mo₆ cluster films was measured by UV-Vis-NIR spectroscopy (V570, Jasco Corp., Tokyo, Japan) in the wavelength range of 220–2000 nm at the scan rate of 400 nm/s.

3. Results and Discussion

The EPD process is one of the useful methods to control the thickness of the Mo₆ cluster film on a nanometer scale by changing the applied voltages and deposition time as shown in Figure 3. The optimal parameters of the EPD process were determined based on the transmittance, thickness, and homogeneity of the Mo₆ cluster films. In this study, 15 V was the suitable voltage to produce a good quality Mo₆ film (1.53 μm) (Figure 3a) since the difference in the homogeneity between the central area and the edge line was visually recognized on the surface of the Mo₆ film prepared at the applied voltage of 16 V. At high voltage, the hydrolysis reaction of the H₂O molecules on the electrode strongly occur to form the H₂ gas; it loses the stability of the suspension and effect to the arrangement of the nanoparticles in the film. In addition, the Mo₆ cluster films deposited at the applied voltages of 16 V cracked quicker than the other films. The quality of the Mo₆ films prepared at 15 V for 10, 20, 30, 40, 50 and 60 s was then investigated to determine the most uniform film (Figure 3b). The Mo₆ film with the maximum thickness was obtained at 40 s (~2 μm), but the homogeneity and the light transmittance of the deposited film slightly decreased with the deposition time. The decrease in the thickness beginning at 40 s has been explained in our previous report [31]. It can be suggested that, at 40 s, the 2 μm-thick film acts as a resistance layer which makes a significant reduction of the electric field which affect to the electrophoresis of the free clusters. The charge balance outside the deposition layers is broken by the attraction of the counter cations (Cs⁺) and the Mo₆ cluster will re-dissolve in the suspension. As a result, the critical thickness of the film is obtained at a deposition time of 40 s. In addition, the Mo₆ film obtained for 30 s possesses sufficient thickness with the significant Mo₆ cluster concentration that positively contributes to the optical property. In summary, the optimal Mo₆ thin film fabricated at 15 V and 30 s was selected to investigate the influence of the PDMS coating on the stabilization of the Mo₆ cluster film.

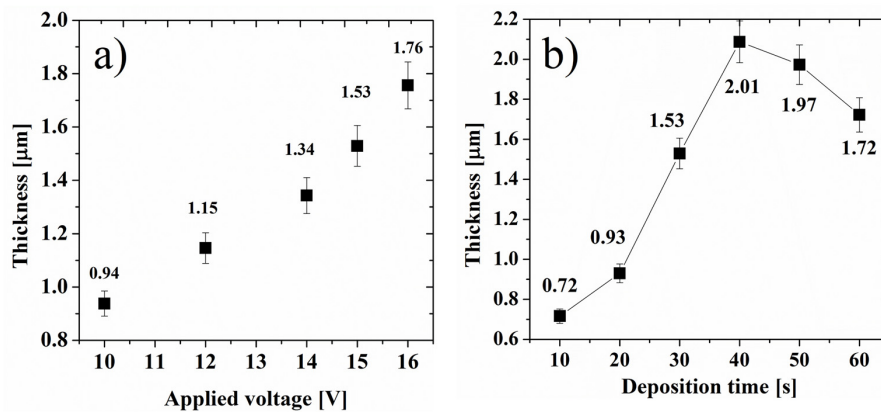


Figure 3. The thickness of the deposited Mo₆ cluster film with hydrophilized-ITO glass versus (a) the applied voltages (fixed for 30 s) and (b) deposition time (fixed at 15 V).

The Mo₆ films prepared by the EPD process at 15 V for 30 s were coated by the PDMS fluids on the surface without any treatment after drying for 10 min. Photos of the PDMS-coated Mo₆ films on the ITO glass with and without hydrophilization are shown in Figure 4. Only the Mo₆ films deposited on the hydrophilized ITO glass followed by coating with the KF-96L-1.5CS and KF-96L-2CS exhibited an insignificant cracking. Most of the other films strongly cracked during drying. Even though, the PDMS-coated films were dried at 40 °C for 7 days, the PDMS fluids containing the viscosity higher than 2 centistokes still existed on the surface of the film accompanying with many flakes that completely separated from the ITO surface. The problems exhibited that the viscosity of the PDMS fluid decided the drying process. The films coated with low-viscosity PDMS fluids obtained volatilized appearance, but the surface of the Mo₆ film was not stable. For this result, the optimal time to coat the PDMS fluid after the EPD process was investigated.

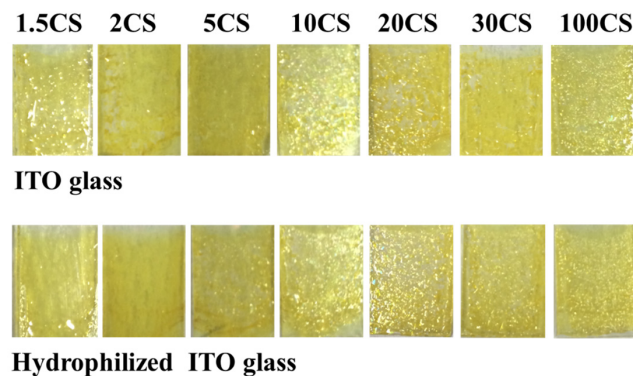


Figure 4. The Mo₆ film deposited on the ITO glass at 15 V for 30 s with or without hydrophilization followed by coating with PDMS of KF-96L-1.5CS, KF-96L-2CS, KF-96L-5CS, KF-96L-10CS, KF-96L-20CS, KF-96L-30CS, and KF-96L-100CS.

Based on these results, KF-96L-1.5CS and KF-96L-2CS were selected to investigate the optimal conditions for the coating because they were dried completely. The Mo₆ film deposited at 15 V for 30 s on the hydrophilized ITO glass were coated with KF-96L-1.5CS or KF-96L-2CS for 0, 30, 60, 90, 120, 150, or 180 min after finishing the EPD (Figure 5). The evaporation speed of the PDMS fluid during drying affects the stabilization of the Mo₆ film. In order to minimize the residual stress during the evaporation, all the films were slowly dried at room temperature for 24 h. The results based on the visual observation of the photos shown in Figure 5 indicated that 90 min after the EPD was the best timing to do the PDMS coating on the surface of the Mo₆ cluster film in order to obtain the highest

stability. The Mo_6 cluster film deposited on the hydrophilized ITO glass followed by the PDMS coating 90 min after the EPD exhibited no cracks or no spalling even after 6 months.

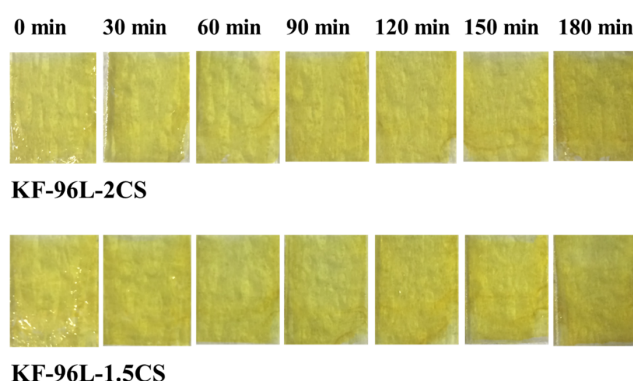


Figure 5. The deposited Mo_6 cluster film at 15 V for 30 s followed by coating the PDMS (KF-96L) with the kinetic viscosity of 1.5 and 2 CS after the different drying times. The photographs of these samples were taken after exposure to the open air for 4 days at room temperature.

The surface appearances of the Mo_6 film, Mo_6 film_1.5CS, and Mo_6 film_2CS samples observed by the color 3D laser microscope and FE-SEM after drying for similar time of 24 h at room temperature are shown in Figure 6. It should be noted that the SEM observation was conducted in a high vacuum. The yellow Mo_6 films seem to be stable despite the appearance of a few hairline cracks in the color 3D laser microscopy images. The stabilization of the films was enhanced after the hydrophilization of the ITO surface. It could be explained that the interaction between the hydrophilic functional groups on the ITO surface and the apical ligands of the octahedral Mo_6 cluster units was slightly improved (Figure 2d), however, the PDMS coating has effectively stabilized the Mo_6 cluster film on the ITO glass surface for a long time. The existence of bubble contamination is recognized by the circular signs on the surface of the Mo_6 film_2CS (Figure 6c (upper)). This problem is not realized in the KF-96L-1.5CS coated Mo_6 film. The KF-96L-2CS has higher viscosity that properly reduce the volatile property at the room temperature. This phenomenon was also observed in the Mo_6 films coated by the PDMS fluids with a kinetic viscosity higher than 2 CS (Figure 4) even dried at 40 °C for 7 days. As displayed in Figure 6 (lower), the Mo_6 film without PDMS appears to have a lot of crack lines, and pieces of the film seem to be separated from the surface of the ITO glass in a high vacuum. In the case of the two PDMS-coated Mo_6 films, a few crack lines were presented, but the deposited film strongly adhered to the surface of the ITO glass.

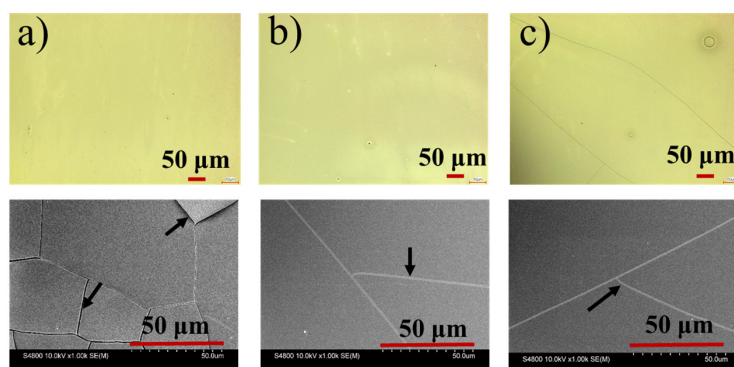


Figure 6. The surface appearance observed by a color 3D microscope (upper) and FE-SEM (lower): (a) Mo_6 film; (b) Mo_6 film_1.5CS; (c) Mo_6 film_2CS.

The Br/Mo atomic ratios of the Mo₆ precursors, Mo₆ film, Mo₆ film_1.5CS, and Mo₆ film_2CS, measured by an EDS measurement are presented in Table 1. These ratios were similar in the coated and un-coated films, which were slightly lower than the ratio of the Cs₂Mo₆Br₈L₆^a cluster precursor. It can be explained that, on average, one (theoretical index Br/Mo ratio, $R = 2.33$) apical Br atom is replaced by solvent molecule or an OH⁻ group originating from the solvents or water involved in the MEK or PDMS during the dissolution. It should be mentioned that the Cs⁺ cations were not detected in all the Mo₆ films without or with the PDMS probably due to the migration of the dissociated Cs⁺ toward the cathode, the counter electrode, during the EPD. This phenomenon has been similarly demonstrated in a previous study [31]. Based on this result, the chemical structure of the Mo₆ film would be [Mo₆Br₈ⁱBr_{6-x}^a(solvent)_x]^{x-2} in the case of the Br ligands replaced by solvent or [Mo₆Br₈ⁱBr_{6-x}^a(OH)_x]²⁻ in the case of the Br ligands replaced by the OH⁻ groups, or [Mo₆Br₈ⁱBr_{6-x}^a(OH)_x(solvent)_a]¹⁻ in the case of the Br ligands replaced by solvent and OH⁻ groups [32]. Moreover, in the anodic EPD process, the Mo₆ cluster units are necessary to have negative charges in order to move toward the anode. It is suggested that the [Mo₆Br₈ⁱBr_{6-x}^a(OH)_x]²⁻ cluster units prior to depositing on the ITO glass are neutralized by the H₃O⁺ cations which are generated from the oxidizing reaction of the H₂O molecules with the surface of the anode. Moreover, a previous study reported that the Mo₆Br₈ⁱBr₄^a·2H₂O cluster units are relatively stable in the solution [36]. The prediction of the transformation from the (H₃O)₂ [Mo₆Br₈ⁱBr_{6-x}^a(OH)_x]^a cluster units to the Mo₆Br₈ⁱBr₄^a·2H₂O cluster units will be carefully demonstrated in a separate publication [32].

Table 1. The Br/Mo atomic ratio and the thickness of the Mo₆ precursor and the deposited Mo₆ film at 15 V for 30 s evaluated by EDX measurement.

Samples	Br/Mo Atomic Ratio (at.% Br/at.% Mo) Theoretical Index of 2.33 (14Br/6Mo)	Thickness (μm)
Mo ₆ precursor	2.29	–
Mo ₆ film	2.20	1.53 ± 0.09
Mo ₆ film_1.5CS	2.21	1.49 ± 0.07
Mo ₆ film_2CS	2.17	1.54 ± 0.08

Most importantly, the PDMS coating on the surface of the Mo₆ cluster film does not significantly affect the thickness of the original Mo₆ film. At the beginning of the investigation, it can be seen that the PDMS coated Mo₆ film still retains its thickness and the Br/Mo atomic ratio of the original Mo₆ cluster deposited film, suggesting the penetration of the PDMS into the cluster layer.

The XRD patterns of the bare ITO glass, the Cs₂Mo₆Br₈ⁱBr₆^a cluster precursor, the Mo₆ film without and with the PDMS coating are shown in Figure 7. The curve of the Cs₂Mo₆Br₈ⁱBr₆^a cluster precursor reveals a good crystallinity with a high intensity of the peaks in the 2θ range of 5° to 35°. The crystallographic structure belonging to the space group of P3c has been reported for the Cs₂Mo₆Br₁₄ cluster precursor [35]. The assignment for the plane in the Cs₂Mo₆Br₁₄ cluster structure that has been confirmed by Saito et al. [37] is presented in Figure 7. The XRD patterns of the Mo₆ film after the EPD retain essentially broad peaks at the 2θ angles of 11° (101) and 30° (114 and 300) without and with the PDMS coating. The grain size calculated from the Scherrer equation at 2θ angle of 11° (101) in the Mo₆ cluster film is approximately 4 nm. The 6-nm cluster nanoparticles was also evidenced by STEM measurement in previous work [31]. Therefore, the broad peaks normally originate from the frameworks of the crystals consisting of by [Mo₆Br₈ⁱBr₆^a]²⁻ cluster units on a nanometer scale, which means the crystal networks of the Cs₂Mo₆Br₈ⁱBr₆^a clusters are rearranged to form new 3D networks due to the disappearance of the Cs⁺ cations. Interestingly, the existence of the PDMS does not have a significant influence on the available crystal networks in the Mo₆ film.

The FTIR spectra of the Mo₆ film, Mo₆ film_1.5CS, Mo₆ film_2CS samples are presented in Figure 8. All spectra similarly display the absorption band of O–H stretching vibration in the wavenumber range from 3600 to 3200 cm⁻¹, simultaneously, the H–O–H bending mode at 1590, 1400 and 794 cm⁻¹ ascribed to the free H₂O molecules and hydrogen bond [32]. These absorption bands originates from

O–H groups linking with the Mo_6 cluster as apical ligands and the H_3O^+ cations absorbing on the surface of the Mo_6 clusters in order to neutralize the negative charge. However, the absorption intensity of O–H stretching vibration at 3550 cm^{-1} indicating free H_2O molecules visibly reduces in the curve of the PDMS-coated Mo_6 films. Interestingly, the PDMS fluids (1.5 and 2 CS) are volatile during drying the film, but the absorption of Si–O bonds is clearly exhibited as the vibrational band at 1080 cm^{-1} . The intensity of Si–O stretching vibration improved when coated with the PDMS owning higher viscosity. Normally, PDMS fluids with low viscosity are almost volatile at room temperature. It can be explained that the PDMS fluid remained in the Mo_6 film after finishing the dry process with a strong interaction by hydrogen bonds or chemical linking with the O–H group or H_2O molecules of the Mo_6 cluster film that forms a new crosslinking network.

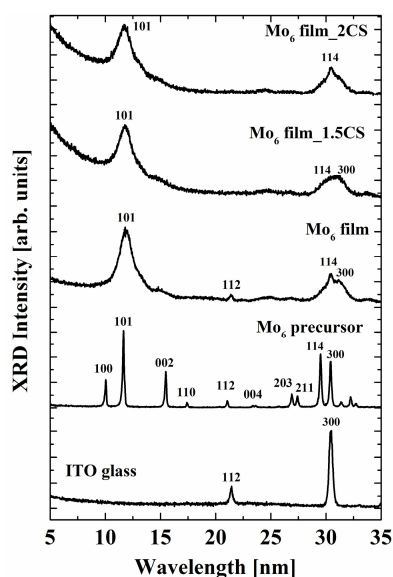


Figure 7. The XRD patterns of the ITO glass, the Mo_6 precursor, and the EPD deposits: Mo_6 film; Mo_6 film_1.5CS; and Mo_6 film_2CS samples.

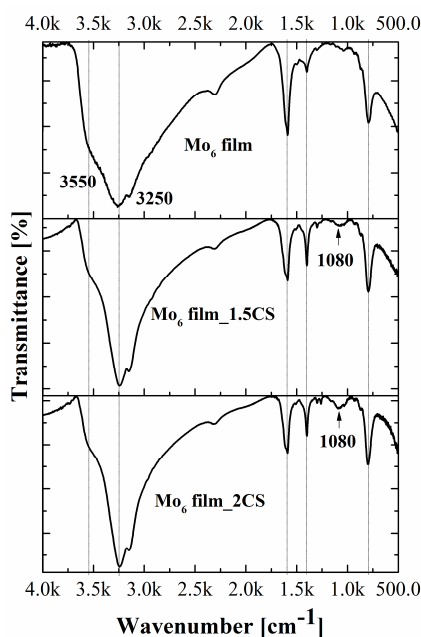


Figure 8. The FT-IR spectrum of the Mo_6 film, Mo_6 film_1.5CS, Mo_6 film_2CS samples.

Some reasons have been suggested to explain the separation of the Mo₆ layers from the ITO glass. The cracking phenomena of the Mo₆ film started to be recognized after 4 days of the dry process at the ambient conditions. The stabilization of the Mo₆ film was partially limited because the evaporation of acetone will create a residual stress, which break the hydrogen bonding between the cluster nanoparticles containing the Mo₆Br₈ⁱBr₄^a·2H₂O and (H₃O)₂ [Mo₆Br₈ⁱBr₄^a (OH)₂^a] cluster units [32] and volume shrinking in the Mo₆ cluster network [38,39]. The cracking point is grown from the tiny grain boundary, which is generated by the separation of the cluster phase and solvent phase.

The PDMS effectively stabilized the morphology of the Mo₆ film in long time under the ambient condition. Indeed, the protective mechanism of the PDMS on the surface of the Mo₆ film have been discussed. In the previous work [32], the main components existing in the Mo₆ film were Mo₆Br₈ⁱBr₄^a·2H₂O and (H₃O)₂ [Mo₆Br₈ⁱBr₄^a (OH)₂^a] cluster units which linked together by hydrogen bonds. Normally, the outside layers of the Mo₆ film mainly contain counter cations as H₃O⁺ to neutralize the [Mo₆Br₈ⁱBr₄^a (OH)₂^a]²⁻ anion. The Mo₆ cluster nanoparticle has functional groups such as H₂O molecule, OH and H₃O⁺ acid group on the surface. During the waiting for 90 min after the EPD, most of the acetone solvent would vaporize, but free water still remains in the deposit layer; it would be the best timing for the PDMS coating, leading to the penetration of the PDMS macromolecules into the grain boundaries of the nanoclusters network. In the acidic condition containing many H₃O⁺ cations absorbed on the surface of the cluster nanoparticles, the Si–O–Si bonds of the PDMS will be decomposed by H₂O molecules with Brønsted acid catalyst (H⁺). The cleavage of the Si–O bonds in siloxane have also been proved in a previous report [40]. Namely, the protective mechanism of the PDMS can be explained as shown in Figure 9: a) in the acid medium, O atom of the ≡Si₁–O–Si₂≡ bond protonated by H⁺ cation creates the electrophile Si₁ atom and ≡Si₂OH and electrophile Si₁ atom coupled with free H₂O molecule to form ≡Si₁–(OH₂)⁺, b) the ≡Si₁–(OH₂)⁺ continually reacts with OH groups of the Mo₆ clusters to form ≡Si₁OH and Mo₆cluster–H₂O, c) the ≡SiOH crosslinks with OH groups of the Mo₆ cluster, d) the hydrogen bond is formed from the ≡SiOH group and the OH or H₂O groups of the Mo₆ cluster accompanying with covalent formed from ≡SiOH group with OH group of the Mo₆ cluster. The new crosslinking network is generated by the short PDMS circuits acting as the bridges between the Mo₆ cluster nanoparticles by covalent and hydrogen bonds. In summary, the crosslinking network prevents the penetration of ambient H₂O and oxygen molecules simultaneously reduces the phase separation at the nanocluster grain boundary and, consequently, improves the stabilization of the Mo₆ network for a long time.

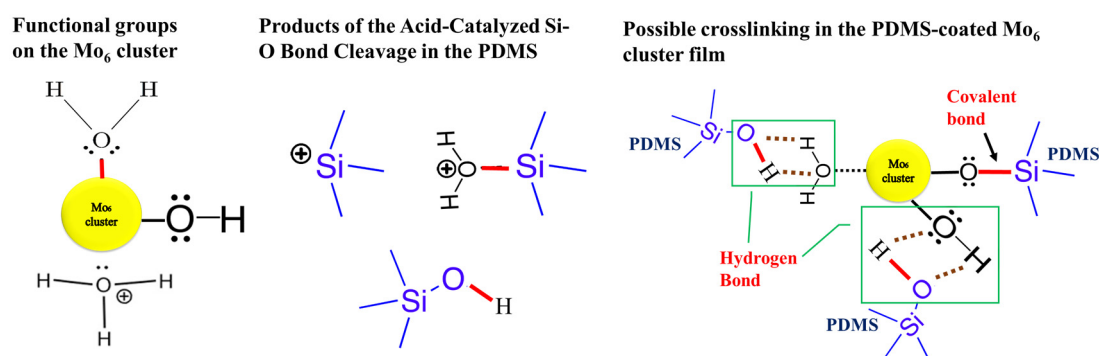


Figure 9. The possible crosslinking mechanism of the PDMS fluid and the Mo₆ cluster nanoparticles under the existence of Brønsted acid catalyst.

UV-Vis absorption is one of the important technique used to evaluate the influence of the PDMS on the Mo₆ film. The absorbance of the Mo₆ precursor in the MEK solution and the transmittance of the ITO glass, Mo₆ film, Mo₆ film_1.5CS, and Mo₆ film_2CS samples are presented in Figure 10. The impressive phenomenon in the UV-Vis-NIR transmittance of the film is the appearance of many peaks in the wavelength range from 600 to 2000 nm that does not exist in the spectra of the ITO glass. The

interference of the incident and reflected lights by the Mo_6 film would give the typical interference pattern [31]. The increase in the number of interference peaks corresponding to the decrease in the distance between the peaks was recognized when the thickness of the transparent and homogeneous Mo_6 film increased. This means that the peaks would disappear if the quality of the Mo_6 film was poor. The Mo_6 precursor strongly absorbs light in the wavelength range of 300 and 500 nm, while the ITO glass absorbs light at wavelengths under 400 nm and NIR higher than 1100 nm. The transmission curves of the Mo_6 film, Mo_6 film_1.5CS and Mo_6 film_2CS samples display strong absorptions in the wavelength range under 580 nm, which is shifted to about a 40 nm higher wavelength compared to the absorption curve of the Mo_6 precursor. This interesting result includes both the absorption by the ITO glass and the Mo_6 clusters in the UV-Vis range. Based on these results, it could be suggested that the new cluster network was formed during the EPD process, which is realized in the XRD pattern, caused the different light absorption of the valance electrons in the energy band gap of the Mo_6 cluster units. The increase of the absorption in the wavelength of visible light would be an advantage for use in UV-Vis light trapping devices. In addition, the absorption intensity in the NIR range of the Mo_6 film is stronger than that of the ITO glass, even if the absorption by the Mo_6 cluster precursor does not exist in this range. Mo_6 cluster film plays an important role in enhancing and retaining the incident light on the surface of the ITO glass by diffraction and reflection between the ITO layers and the top of the Mo_6 film. In summary, the use of the PDMS fluid do not change the optical properties of the Mo_6 film.

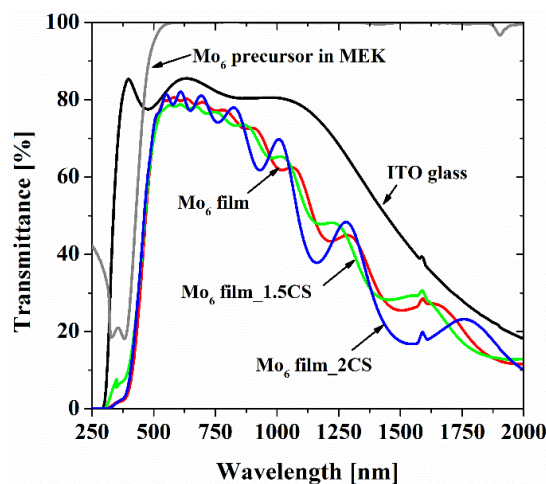


Figure 10. The UV-Vis absorption spectra of the of ITO glass and the Mo_6 precursor, Mo_6 film, Mo_6 film_1.5CS, Mo_6 film_2CS samples.

4. Conclusions

The stabilization of the Mo_6 cluster thin film was improved by the hydrophilization of the surface of the ITO glass and the use of PDMS as a top-coating agent on the surface of the Mo_6 film. The effectiveness of the hydrophilization enhances the good interaction between the first layer of the Mo_6 clusters and ITO layers, while the PDMS prevents the penetration of air and moisture. The results of the study indicated that the thickness, the Br/Mo atomic ratio, surface morphology, crystallographic pattern, chemical linking, and UV-Vis absorption of the Mo_6 film with the PDMS coating were not significantly changed by the PDMS coating. In addition, the KF-96L-1.5CS is the best PDMS because its evaporation is completely on the surface of the Mo_6 film in a short time at room temperature. This combination helps the Mo_6 film retain its stabilization for more than 6 months under ambient conditions. In addition, the protective mechanism of the PDMS fluid towards the Mo_6 film have been discussed by creating a new crosslinking network during the drying process at the ambient condition. The results of this study will be used in an investigation in order to develop an application of the Mo_6 film for a UV-Vis and NIR light trapping window.

Acknowledgments: This study was carried out as part of the France-Japan international collaboration framework through the Laboratory for Innovative Key Materials and Structures (UMI 3629-LINK Center). The study was financially supported by the National Institute for Materials Science (NIMS), Saint-Gobain (France), CNRS and Université de Rennes 1 (UMR 6226). The authors wish to thank David Lechevalier and Mari Kono of Saint-Gobain K.K. (Tokyo, Japan) involved in LINK and related activities. We thank Chenning. Zhang at NIMS for his help with the EPD experiments.

Author Contributions: Thi Kim Ngan Nguyen, Fabien Grasset, and Tetsuo Uchikoshi conceived and designed the experiments; Thi Kim Ngan Nguyen and Tetsuo Uchikoshi performed the experiments; Thi Kim Ngan Nguyen, Tetsuo Uchikoshi, Benjamin Dierre, and Adèle Renaud analyzed the data; Tetsuo Uchikoshi, Hiroshi Fudouzi, Naoki Ohashi, Stéphane Cordier, Pierric Lemoine, and Noée Dumait contributed reagents/materials/analysis tools; Thi Kim Ngan Nguyen, Fabien Grasset, and Tetsuo Uchikoshi wrote the paper.

Conflicts of Interest: The authors declare no conflict of interest. The sponsors had no role in the design of the study; in the collection, analyses, or interpretation of the data; in the writing of the manuscript; or in the decision to publish the results.

References

1. Shang, Q.; Zhou, Y. Fabrication of transparent superhydrophobic porous silica coating for self-cleaning and anti-fogging. *Ceram. Int.* **2016**, *42*, 8706–8712. [[CrossRef](#)]
2. Liang, Z.; Zhao, L.; Meng, W.; Zhong, C.; Wei, S.; Dong, B.; Xu, Z.; Wan, L.; Wang, S. Tungsten-doped vanadium dioxide thin films as smart windows with self-cleaning and energy-saving functions. *J. Alloy. Compd.* **2017**, *694*, 124–131. [[CrossRef](#)]
3. Granqvist, C. Electrochromics for smart windows: Oxide-based thin films and devices. *Thin Solid Films* **2014**, *564*, 1–38. [[CrossRef](#)]
4. Feng, G.; Zou, L.; Gao, G.; Wua, G.; Shena, J.; Li, W. Gasochromic smart window: Optical and thermal properties, energy simulation and feasibility analysis. *Sol. Energy Mater. Sol. Cells* **2016**, *144*, 316–323. [[CrossRef](#)]
5. Dai, J.; Gao, W.; Liu, B.; Cao, X.; Tao, T.; Xie, Z.; Zhao, H.; Chen, D.; Ping, H.; Zhang, R. Design and fabrication of UV band-pass filters based on SiO₂/Si₃N₄ dielectric distributed bragg reflector. *Appl. Surf. Sci.* **2016**, *364*, 886–891. [[CrossRef](#)]
6. Guo, C.; Sun, T.; Cao, F.; Liu, Q.; Ren, R. Metallic nanostructures for light trapping in energy-harvesting devices. *Light Sci. Appl.* **2014**, *3*, 161–173.
7. Cordier, S.; Kirakci, K.; Méry, D.; Perrin, C.; Astruc, D. Mo₆X₈ⁱ Nanocluster Cores (X: Br, I): From inorganic solid state compounds to hybrids. *Inorg. Chim. Acta* **2006**, *359*, 1705–1709. [[CrossRef](#)]
8. Cordier, S.; Grasset, F.; Molard, Y.; Amela-Cortes, M.; Boukherroub, R.; Ravaine, S.; Mortier, M.; Ohashi, N.; Saito, N.; Haneda, N. Inorganic molybdenum octahedral nanosized cluster units, versatile functional building block for nanoarchitectonics. *J. Inorg. Organomet. Polym.* **2015**, *25*, 189–204. [[CrossRef](#)]
9. Renaud, A.; Grasset, F.; Dierre, B.; Uchikoshi, T.; Ohashi, N.; Takei, T.; Planchat, A.; Cario, L.; Jobic, S.; Odobel, F.; et al. Inorganic molybdenum clusters as light-harvester in all inorganic solar cells: A proof of concept. *Chem. Sel.* **2016**, *1*, 2284–2289. [[CrossRef](#)]
10. Zhao, Y.; Lunt, R.R. Transparent luminescent solar concentrators for large-area solar windows enabled by massive stokes-shift nanocluster phosphors. *Adv. Ener. Mater.* **2013**, *3*, 1143–1148. [[CrossRef](#)]
11. Kuttipillai, P.S.; Zhao, Y.; Traverse, C.J.; Staples, R.J.; Levine, B.G.; Lunt, R.R. Light-emitting diodes: Phosphorescent nanocluster light-emitting diodes. *Adv. Mater.* **2016**, *28*, 319. [[CrossRef](#)] [[PubMed](#)]
12. Kumar, P.; Kumar, S.; Cordier, S.; Paofai, S.; Boukherroub, R.; Jain, S. Photoreduction of CO₂ to methanol with hexanuclear molybdenum [Mo₆Br₁₄]²⁻ cluster units under visible light irradiation. *RSC Adv.* **2014**, *4*, 10420–10423. [[CrossRef](#)]
13. Mitzi, D.B.; Schwartz, R.W.; Narayanan, M. *Solution Processing of Inorganic Materials*; Mitzi, D.B., Ed.; John Wiley & Sons, Inc.: Etobicoke, Toronto, ON, Canada, 2008; Volume 2, pp. 33–76.
14. Schneller, T.; Waser, R.; Kosec, M.; Payne, D. *Chemical Solution Deposition of Functional Oxide Thin Films*; Springer Science & Business Media: Aachen, Germany, 2014; pp. 233–319.
15. Willmott, P.R.; Huber, J.R. Pulsed laser vaporization and deposition. *Rev. Mod. Phys.* **2000**, *72*, 315–328. [[CrossRef](#)]
16. Gondoni, P.; Ghidelli, M.; Fonzo, D.F.; Bassi, A.L.; Casari, C.S. Fabrication of nano-engineered transparent conducting oxides by pulsed laser deposition. *J. Vis. Exp.* **2013**, *72*, 50297. [[CrossRef](#)] [[PubMed](#)]

17. Gondoni, P.; Ghidelli, M.; Fonzo, F.D.; Russo, V.; Bruno, P.; Martí-Rujas, J.; Bottani, C.E.; Bassi, A.L.; Casari, C.S. Highly performing Al: ZnO thin films grown by pulsed laser deposition at room temperature. *Nanosci. Nanotechnol. Lett.* **2013**, *5*, 484–486. [[CrossRef](#)]
18. Tabellion, J.; Clasen, R. Electrophoretic deposition from aqueous suspensions for near-shape manufacturing of advanced ceramics and glasses-applications. *J. Mater. Sci.* **2004**, *39*, 803–811. [[CrossRef](#)]
19. Boccaccini, A.; Peters, C.; Roether, J.; Eifler, D.; Misra, S.; Minay, S. Electrophoretic deposition of polyetheretherketone (PEEK) and PEEK/Bioglass coatings on NiTi shape memory alloy wires. *J. Mater. Sci.* **2006**, *41*, 8152–8159. [[CrossRef](#)]
20. Yoshioka, T.; Chávez-Valdez, A.; Roether, J.; Schubert, D.; Boccaccini, A. AC electrophoretic deposition of organic–inorganic composite coatings. *J. Colloid Interface Sci.* **2013**, *392*, 167–171. [[CrossRef](#)] [[PubMed](#)]
21. Guo, X.; Li, X.; Li, H.; Zhang, D.; Lai, C.; Li, W. A Comprehensive investigation on the electrophoretic deposition (EPD) of Nano-Al/Ni energetic composite coatings for the combustion application. *Surf. Coat. Technol.* **2015**, *265*, 83–91. [[CrossRef](#)]
22. Besra, L.; Liu, M. A review on fundamentals and applications of electrophoretic deposition (EPD). *Prog. Mater. Sci.* **2007**, *52*, 1–61. [[CrossRef](#)]
23. Corni, I.; Ryan, M.; Boccaccini, A.A. Electrophoretic deposition: From traditional ceramics to nanotechnology. *J. Eur. Ceram. Soc.* **2008**, *28*, 1353–1367. [[CrossRef](#)]
24. Diba, M.; Fam, D.; Boccaccini, A.; Shaffer, M. Electrophoretic deposition of graphene-related materials: A review of the fundamentals. *Prog. Mater. Sci.* **2016**, *82*, 83–117. [[CrossRef](#)]
25. Acevedo-Peña, P.; González, I. TiO₂ photoanodes prepared by cathodic electrophoretic deposition in 2-propanol: Effect of the electric field and deposition time. *J. Solid State Electrochem.* **2013**, *17*, 519–526. [[CrossRef](#)]
26. Cordero-Arias, L.; Cabanas-Polo, S.; Goudouri, O.; Misra, S.; Gilabert, J.; Valsami-Jones, E.; Sanchez, E.; Virtanen, S.; Boccaccini, A. Electrophoretic deposition of ZnO/alginate and ZnO-bioactive glass/alginate composite coatings for antimicrobial applications. *Mater. Sci. Eng. C* **2015**, *55*, 137–144. [[CrossRef](#)] [[PubMed](#)]
27. Fiorilli, S.; Baino, F.; Crepaldi, M.; Demarchi, D.; Cauda, V.; Vitale-Brovarone, C.; Onida, B. Electrophoretic deposition of mesoporous bioactive glass on glass–ceramic foam scaffolds for bone tissue engineering. *J. Mater. Sci. Mater. Med.* **2015**, *26*, 21. [[CrossRef](#)] [[PubMed](#)]
28. Meng, D.; Francis, L.; Boccaccini, A. Using electrophoretic deposition to identify protein charge in biological medium. *J. Appl. Electrochem.* **2011**, *41*, 919–923. [[CrossRef](#)]
29. Clavijo, S.; Membrives, F.; Quiroga, G.; Boccaccini, A.; Santillán, M. Electrophoretic deposition of chitosan/Bioglass[®] and chitosan/Bioglass[®]/TiO₂ composite coatings for bioimplants. *Ceram. Int.* **2016**, *42*, 14206–14213. [[CrossRef](#)]
30. Truong, G.; Dierre, B.; Grasset, F.; Saito, N.; Saito, N.; Nguyen, N.; Takahashi, K.; Uchikoshi, T.; Amela-Cortes, M.; Molard, Y.; et al. Visible tunable lighting system based on polymer composites embedding ZnO and metallic clusters: From colloids to thin films. *Sci. Technol. Adv. Mater.* **2016**, *17*, 443–453. [[CrossRef](#)] [[PubMed](#)]
31. Nguyen, N.; Grasset, F.; Dierre, B.; Matsunaga, C.; Cordier, S.; Lemoine, P.; Ohashi, N.; Uchikoshi, T. Fabrication of transparent thin film of octahedral molybdenum metal clusters by electrophoretic deposition. *ECS J. Solid State Sci. Technol.* **2016**, *5*, 178–186. [[CrossRef](#)]
32. Nguyen, T.K.N.; Dierre, B.; Grasset, F.; Renaud, A.; Cordier, S.; Lemoine, P.; Ohashi, N.; Uchikoshi, T. Formation mechanism of transparent Mo₆ metal atom cluster film prepared by electrophoretic deposition. *J. Electrochem. Soc.* **2017**, *164*, 412–418. [[CrossRef](#)]
33. Gray, H.B.; Maverick, A.W. Solar chemistry of metal complexes. *Science* **1981**, *214*, 1201–1205. [[CrossRef](#)] [[PubMed](#)]
34. Seethapathy, S.; Górecki, T. Applications of polydimethylsiloxane in analytical chemistry: A review. *Anal. Chim. Acta* **2012**, *750*, 48–62. [[CrossRef](#)] [[PubMed](#)]
35. Kirakci, K.; Cordier, S.; Perrin, C. Synthesis and characterization of Cs₂Mo₆X₁₄ (X = Br or I) hexamolybdenum cluster halides: Efficient Mo₆ cluster precursors for solution chemistry syntheses. *Z. Anorg. Allg. Chem.* **2005**, *631*, 411–416. [[CrossRef](#)]
36. Guggenberger, L.; Sleight, A. Structural and bonding characterizations of molybdenum dibromide, Mo₆Br₁₂·2H₂O. *Inorg. Chem.* **1969**, *8*, 2041–2049. [[CrossRef](#)]

37. Saito, N.; Cordier, S.; Lemoine, P.; Ohsawa, T.; Wada, Y.; Grasset, F.; Cross, S.J.; Ohashi, N. Lattice and valence electronic structures of crystalline octahedral molybdenum halide clusters-based compounds, $\text{Cs}_2[\text{Mo}_6\text{X}_{14}]$ ($\text{X} = \text{Cl}, \text{Br}, \text{I}$), studied by density functional theory calculations. *Inorg. Chem.* **2017**, *56*, 6234–6243. [[CrossRef](#)] [[PubMed](#)]
38. Engwall, A.M.; Rao, Z.; Chason, E. Origins of residual stress in thin films: Interaction between microstructure and growth kinetics. *Mater. Des.* **2016**, *110*, 616–623. [[CrossRef](#)]
39. Ghidelli, M.; Sebastiani, M.; Collet, C.; Guillemet, R. Determination of the elastic moduli and residual stresses of freestanding Au-TiW bilayer thin films by nanoindentation. *Mater. Des.* **2016**, *106*, 436–445. [[CrossRef](#)]
40. Cypryk, M.; Apeloig, Y. Mechanism of the Acid-Catalyzed Si–O bond cleavage in siloxanes and siloxanols: A theoretical study. *Organometallics* **2002**, *21*, 2165–2175. [[CrossRef](#)]



© 2017 by the authors. Licensee MDPI, Basel, Switzerland. This article is an open access article distributed under the terms and conditions of the Creative Commons Attribution (CC BY) license (<http://creativecommons.org/licenses/by/4.0/>).